



RESEARCH ARTICLE

Extremely powerful and frequency-tunable terahertz pulses from a table-top laser–plasma wiggler

Jie Cai¹, Yinren Shou³, Yixing Geng¹, Liqi Han², Xinlu Xu¹, Shuangchun Wen², Baifei Shen⁴, Jinqing Yu², and Xueqing Yan^{1,5,6}

¹State Key Laboratory of Nuclear Physics and Technology, and Key Laboratory of HEDP of the Ministry of Education, CAPT, Peking University, Beijing, China

²Hunan Provincial Key Laboratory of High-Energy Scale Physics and Applications, School of Physics and Electronics, Hunan University, Changsha, China

³Center for Relativistic Laser Science, Institute for Basic Science, Gwangju, Republic of Korea

⁴Shanghai Normal University, Shanghai, China

⁵Collaborative Innovation Center of Extreme Optics, Shanxi University, Taiyuan, China

⁶Guangdong Laser Plasma Institute, Guangzhou, China

(Received 13 June 2023; revised 25 July 2023; accepted 18 September 2023)

Abstract

The production of broadband, terawatt terahertz (THz) pulses has been demonstrated by irradiating relativistic lasers on solid targets. However, the generation of extremely powerful, narrow-band and frequency-tunable THz pulses remains a challenge. Here, we present a novel approach for such THz pulses, in which a plasma wiggler is elaborated by a table-top laser and a near-critical density plasma. In such a wiggler, the laser-accelerated electrons emit THz radiations with a period closely related to the plasma thickness. The theoretical model and numerical simulations predict that a THz pulse with a laser–THz energy conversion of over 2.0%, an ultra-strong field exceeding 80 GV/m, a divergence angle of approximately 20° and a center frequency tunable from 4.4 to 1.5 THz can be generated from a laser of 430 mJ. Furthermore, we demonstrate that this method can work across a wide range of laser and plasma parameters, offering potential for future applications with extremely powerful THz pulses.

Keywords: laser; plasma; terahertz; wiggler

1. Introduction

Terahertz (THz) waves^[1], which are significantly less developed and utilized than microwaves and light waves, used to be regarded as the ‘THz gap’^[2] in the electromagnetic spectrum due to the limitations of traditional electronic or optical methods in producing terahertz radiation during the early years. Such THz pulses have attracted significant interest for their potential applications in fields such as biology, medicine, material science, optical communication and the military^[3–8]. To generate THz waves, several

routine methods, such as cascade quantum laser^[9,10], optical rectification^[11,12], photoconductive^[13] and vacuum electronic^[14,15] methods, have been widely demonstrated. Due to the material damage threshold, these methods are incapable of generating extremely powerful THz pulses. Such pulses can be used as a powerfully driven pulse for probing and controlling material properties^[16,17], biological macromolecules^[4], electron beam detection^[18] and charged particle acceleration^[19,20]. For instance, the mechanisms of four-wave mixing and photoionization become saturated in under-dense plasma just around the power of 10^{15} W/cm²^[21–23]. As laser intensity continues to improve and nanotechnology develops, terahertz sources based on ultra-intense laser irradiation of dense plasma have started to emerge^[24,25].

During the past two decades, the quick development of relativistic laser systems, whose peak intensity

Correspondence to: Jinqing Yu, Hunan Provincial Key Laboratory of High-Energy Scale Physics and Applications, School of Physics and Electronics, Hunan University, Changsha 410082, China. Email: jinqing.yu@hnu.edu.cn; Xueqing Yan, State Key Laboratory of Nuclear Physics and Technology, and Key Laboratory of HEDP of the Ministry of Education, CAPT, Peking University, Beijing 100871, China. Email: x.yan@pku.edu.cn

exceeds 10^{18} W/cm², has opened a new door to obtain extremely powerful THz pulses^[26]. However, the existing terahertz sources based on relativistic lasers lack the ability to tune their spectra, which limits their versatility in applications^[20,27–30]. For example, two-color laser filaments can produce THz pulses with field amplitudes above 10 GV/m and a conversion efficiency of 2.36%^[31], but such pulses have a non-tunable center frequency and a large bandwidth around hundreds of GHz. Another novel method, coherent transition radiation (CTR), occurs when an overdense electron bunch, produced by irradiating a relativistic laser on a solid target, passes through the vacuum–plasma interface and can emit THz pulses with an energy of 55 mJ and a peak electron field at 4 GV/m^[32]. Numerous efforts have been dedicated to achieving tunable strong-field terahertz radiation using various approaches, such as plasma oscillation^[33–35] and plasma slab methods^[36]. However, most of these solutions have not been able to reach high field strengths. Miao *et al.*^[34] demonstrated frequency-tunable terahertz radiation with weak field strength by manipulating the frequency of plasma waves. Kwon *et al.*^[35] developed a terahertz source based on plasma dipole oscillation formed by two laser pulses. One of the challenges lies in accessing terahertz frequencies through radiation from plasma waves, as it requires extremely low densities, making it difficult to obtain strong-field terahertz radiation simultaneously. In a significant breakthrough, Liao *et al.*^[37] achieved 0.1–1 THz tunable radiation by transforming the terahertz generation mechanism in laser-irradiated solid targets. However, it should be noted that the radiation derived from different mechanisms exhibits distinct characteristics. The center frequency of strong-field terahertz radiations above 1 THz from CTR is also non-adjustable^[38].

Here, we propose a novel plasma wiggler that uses a femtosecond (fs) laser pulse to produce frequency-tunable and extremely powerful terahertz radiations, improving the flexibility and accuracy of terahertz applications. Figure 1(a) draws the concept of the plasma wiggler. A laser pulse is used to irradiate a block-shaped near-critical density plasma, producing hot electrons^[39]. The accelerated electrons move in two different trajectories. One kind of high-energy electrons gets rid of the potential barrier of the surface electric field and goes away from the plasma surface. The other group of electrons is trapped by the barrier acting as a wiggler. Figure 1(b) illustrates the laser–plasma interaction snapshot at around 273 fs. When this electron beam passes through the transverse interfaces of the plasma, THz radiation^[38] and sheath fields E_s ^[40] can be induced near the interfaces. Under the influence of E_s , the electrons are pulled back into the plasma and cross the transverse interface on the other side, exhibiting reciprocating motion along the plasma. The period of this motion is closely related to the plasma thickness and the size of E_s . As a result, the plasma with transverse sheath fields E_s can be used as a wiggler to

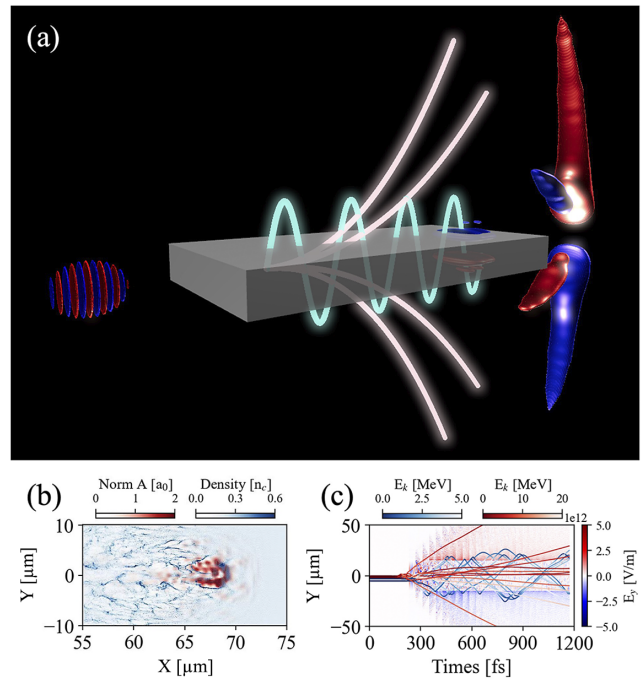


Figure 1. (a) Schematic for the generation of a high-power, collimated, narrow-band and center-frequency-tunable THz pulse. An intense femtosecond laser pulse irradiates on the left-hand side of a block-shaped near-critical density plasma. Hot electrons generated by laser ponderomotive force can be separated into two groups: the electrons in group A moving forward leaving the plasma and the electrons in group B reciprocating under the sheath fields E_s ; here the transverse sheath fields E_s are induced when electrons pass through the plasma transverse interfaces. Under the action of E_s , electrons in group B could be pulled back into the plasma and pass through the transverse interface on the other side. Such wiggler-like motions of these electrons can emit the desired THz pulse. (b) The electron accelerating in the plasma. (c) The trajectories of the two groups of electrons (blue and red) in the surface charge separation field.

manipulate the reciprocating motion of the electrons and regulate THz radiations. A theoretical model, which is verified by particle-in-cell (PIC) simulations, has been developed to describe the physical principles of the tunable THz pulse generation.

Based on the theoretical model and PIC simulations, we find that the center frequency of the THz pulse can be regulated by changing the thickness of the plasma. In simulations using a laser pulse with energy of approximately 430 mJ, the generated THz pulse has a divergence angle of approximately 20° , an ultra-strong-field strength of over 80 GV/m, a laser–THz conversion efficiency of over 2.0% and a center frequency tunable from 4.4 to 1.5 THz by varying the plasma thickness from 20 to 80 μm . We also demonstrate that this plasma wiggler can work effectively over a wide range of plasma length, thickness, density and laser intensity. Therefore, this method could overcome significant scientific obstacles in the generation of high-quality THz sources and open up brand-new applications^[27–31].

2. Results

2.1. Theoretical model and simulation setup

When an intense laser pulse irradiates on a plasma, as shown in Figure 1(b), hot electrons whose beam length is close to the laser duration can be generated by laser ponderomotive force^[39]. The electron beam transports in the plasma and passes through its transverse interfaces. As a result, transverse sheath fields E_s (more details in the Supplementary Material) can be generated and the maximum strength^[40] on the plasma surfaces can be expressed as follows:

$$E_s = \sqrt{\frac{8\pi n_e T_e}{e}}, \quad (1)$$

where e is the Euler's number and n_e and T_e are the density and temperature of the hot electrons, respectively. Here, transverse sheath fields E_s higher than 10^{12} V/m can be induced near the plasma transverse interfaces^[41], as shown in Figure 1(c). Under the action of E_s , electrons whose kinetic energy is less than ε_e could be pulled back into the plasma and pass through the transverse interface on the other side^[42], where ε_e could be calculated by the following:

$$\varepsilon_e = \int_0^{l_e} \frac{E_s}{\sin\phi} dl. \quad (2)$$

Here, l is the transverse size of E_s , ϕ is the angle at which the electron enters the transverse sheath fields E_s and l_e is the transverse location where the electron could be pulled back into the plasma. An electron field derived from the simulation was used (more details in the Supplementary Material) for calculation, and then the relation between ε_e and l_e could be plotted in Figure 2 by employing E_s as shown in Figure 1(c). In the case that the electron perpendicularly penetrates E_s ($\phi = 90^\circ$), the threshold kinetic energy is about 6 MeV. Most of the electrons penetrate the transverse sheath fields with a much smaller ϕ , and the threshold kinetic energy could be much higher than 6 MeV. Some electrons, which are located in the forefront of the electron beam and experienced much weaker E_s , could not be pulled back to the plasma even with a much smaller kinetic energy^[43]. According to the large difference in the dynamical behavior of the hot electrons, as shown in Figure 1(c) with red and blue colors, we could separate the hot electrons into two groups: the electrons in group A located in the front of the electron beam are marked with a red color and the electrons in group B located in the beam rear express are marked with a blue color.

Here, E_s , which propagates along the plasma surface^[44] at a velocity close to light speed, can guide the hot electrons in group B to oscillate transversely and propagate longitudinally, as shown in Figure 1(c). Every time the electron

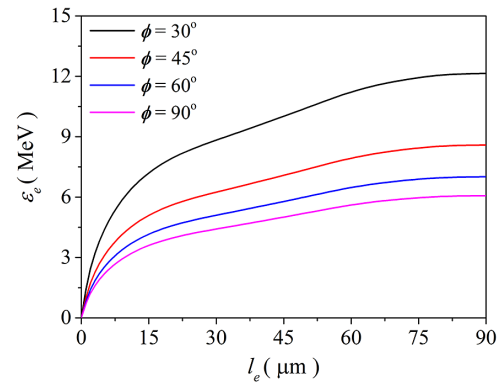


Figure 2. In the case of the electron penetrating E_s with different ϕ (the angle at which the electron enters E_s), the relation between the electron threshold kinetic energy ε_e and the transverse location l_e where the electron could be pulled back into the plasma.

passes through the transverse interfaces of the plasma, THz radiation can be emitted. This behaves like a wiggler in traditional light sources^[45]. Therefore, the plasma with transverse sheath fields E_s can be considered as a wiggler for the electrons in group B. The reciprocating (wiggler) period of the electron can be expressed as follows:

$$\tau_r = \frac{4l_s + 2l_t}{v_t}. \quad (3)$$

Here, l_s is the transverse distance between the plasma interface and the point where the electron turns around, l_t is the thickness of the plasma and v_t is the median transverse velocity of the electrons; l_s is determined by the transverse momentum of electrons and the strength of E_s . The radiation frequency f is closely related to the wiggler frequency $f_w = 1/\tau_r$, and then we have the following:

$$f = \frac{f_w (2\gamma^2)}{1 + K^2/2} = \frac{v_t (2\gamma^2)}{(4l_s + 2l_t) (1 + K^2/2)}, \quad (4)$$

where γ is the electron Lorentz factor and K is the wiggle (undulator) parameter^[46]. Normally, l_s is several micrometers^[43]; while the changes in γ , K and v_t can be ignored for the same laser intensity and plasma density, then l_t is the only parameter that could be varied. Hence, one can regulate the frequency of the THz radiation by changing the plasma thickness l_t according to Equation (4). Since the length of the electron beam is close to the laser pulse duration, which is only 32 fs here, the radiation satisfies the time coherence condition at the THz frequencies^[32].

2.2. Electron kinetics

To generate electrons in group B, one should use a plasma with limited transverse size to ensure the occurrence of reciprocating motion. Simulations, with plasma of different

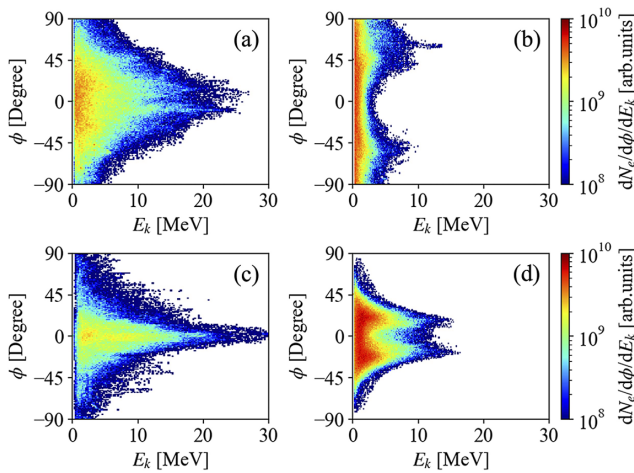


Figure 3. The angular-spectra distribution of the hot electrons. The electrons from a plasma length of $l_p = 50 \mu\text{m}$ (a) collected by a screen with a radius of $55 \mu\text{m}$ in the first 270 fs of the simulation could be classified to group A, and (b) the electrons behind group A can be assigned to group B. The electrons from a plasma length of $l_p = 200 \mu\text{m}$ (c) in group A collected by a screen whose radius is $205 \mu\text{m}$ in the first 770 fs and (d) the electrons in group B.

lengths l_p (fixing the plasma thickness l_t to $30 \mu\text{m}$), were performed to see the effect of plasma length on the electron dynamics. From the simulations with $l_p \geq 50 \mu\text{m}$, it was found that more than 75% of the laser energy was converted to hot electrons (electron kinetic energy $e_k \geq 0.5 \text{ MeV}$). Meanwhile, in the case of $l_p = 10 \mu\text{m}$, there were few electrons participating in reciprocating motion and most of the electrons could be classified into group A.

When l_p was increased to $50 \mu\text{m}$, one could easily distinguish the electrons in group B from those in group A, as plotted in Figures 3(a) and 3(b). Figure 3(a) shows a typical angular-spectra distribution of the electrons, with a large divergence angle, accelerated by the laser ponderomotive force^[39]. This figure is very similar to the result of $l_p = 10 \mu\text{m}$. Under the action of E_s , the reciprocating motion of the electrons is facilitated and obvious changes in the angular-spectra distribution can be seen in Figure 3(b). In this case, the electron beam had a divergence angle of approximately 60° , which indicates that most of the electrons penetrate the transverse sheath fields with an angle of $\phi \approx 60^\circ$. Hence, the threshold kinetic energy of the electron ε_c is about 8 MeV, which is consistent with the theoretical value predicted by Equation (2), as shown in Figure 2. If l_p is further increased, such as $l_p = 200 \mu\text{m}$, more electrons of relatively low energy in group A come into group B, as shown in Figure 3(c), and the number of electrons in group B increases with l_p . As a result, the electron number shown in Figure 3(d) is larger than that in Figure 3(b). It is noted that the electrons in group B were manipulated and collimated into a smaller divergence angle by E_s , and the electron threshold kinetic energy ε_c could be much higher, as predicted by Equation (2).

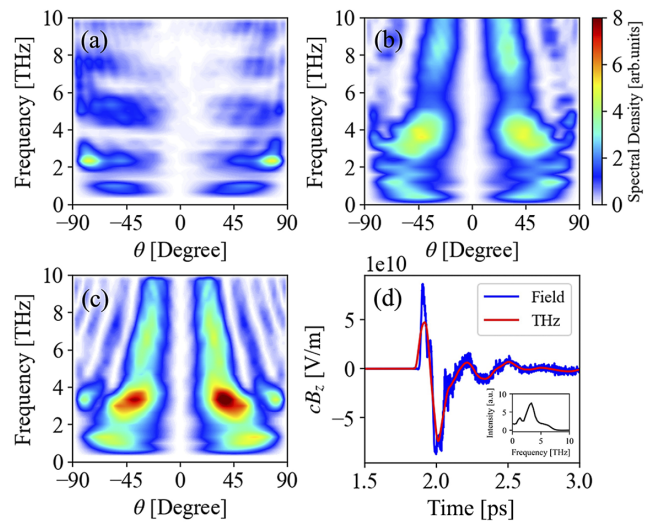


Figure 4. Simulation results from the plasma of different lengths l_p , while the thickness l_t was fixed to $30 \mu\text{m}$. The angular-spectra distribution of the THz pulses from (a) $l_p = 50 \mu\text{m}$, (b) $l_p = 150 \mu\text{m}$ and (c) $l_p = 300 \mu\text{m}$. (d) The radiation field before filtering (blue line) and the field of the THz pulse (red line) collected at 37° from the simulation of $l_p = 300 \mu\text{m}$.

We used a semicircular receiving screen, whose radius was $250 \mu\text{m}$ with the center locating at the midpoint of the plasma right-hand interface, to collect the radiation field. Then, the angular-spectra distribution of the THz source could be obtained from the radiation field through Fourier transform^[47]. In this work, the angular spectrum method^[47–49] was employed to remove the near-field radiation, and then all the results of the THz source could be recognized as far-field radiation.

In the simulation with $l_p = 150 \mu\text{m}$, the median longitudinal (transverse) velocity v_l (v_t) of the electrons in group B was $0.94c$ ($0.85c$). The transverse size of E_s was about $2 \mu\text{m}$ (at full width at half maximum (FWHM)), and therefore we could assume $l_s \approx 2 \mu\text{m}$. According to Equation (3), one can get $\tau_r = 270 \text{ fs}$ and $\lambda_w \approx \tau_r \times v_l = 79.4 \mu\text{m}$. The wiggler period $\tau_w = \tau_r$ corresponds to a wiggler frequency $f_w = 3.7 \text{ THz}$, and the Lorentz factor γ for the longitudinal velocity v_l was 2.93. By tracking the electromagnetic fields exerting on the electrons in group B, we got an average value of $K \approx 6.0$, which decreased to 5.5 when l_s increased to $80 \mu\text{m}$. According to Equation (4), the radiation frequency was $f = 3.34 \text{ THz}$, which is also the same as the center frequency of 3.35 THz from the simulation. Hence, the theoretical model can accurately predict the terahertz frequency obtained from the simulations.

2.3. Spectrum of terahertz pulses

Figures 4(a)–(c) show the angular-spectra distribution of the THz pulses from the plasma lengths $l_p = 50, 150$ and $300 \mu\text{m}$. In the condition of l_p being shorter than λ_w , the

role of the electrons in group B could be ignored and the generation of the THz source is dominated by target rear CTR^[32,37,50] from the electrons in group A. Hence, the THz source had a large divergence angle (pointed at 88°) and a small energy conversion efficiency of 0.45%, as shown in Figure 4(a).

Every time the electron passes through the transverse interfaces of the plasma, THz radiation can be emitted and becomes stronger in the case of the electrons in group B oscillating for several periods. When l_p was enlarged to $150\ \mu\text{m}$, more than 1.3% of the laser energy was converted to THz radiation and the characteristics of the narrow spectrum became obvious, as shown in Figure 4(b). The simulation results indicated that $l_p \geq 150\ \mu\text{m}$ was more conducive to obtain THz pulses of a narrow spectrum, as shown in Figures 4(b) and 4(c). As the electrons in group B are guided to oscillate along the plasma by E_s , the resulting THz pulse could be better collimated than the other intense laser-plasma-based THz sources^[26,37,50]. It was found that the THz pulse that pointed at $\theta = 37^\circ$ could be collimated into a divergence angle of approximately 20° , as shown in Figure 4(c). Since $\theta > 1/\gamma$, we call it a wiggler instead of an undulator. Then we collected the radiation field at 37° from the simulation of $l_p = 300\ \mu\text{m}$, and filtered the THz signal (frequency range: 0.1–10 THz) from the radiation field, as shown in Figure 4(d). The THz field was higher than 80 GV/m, which was much greater than those from THz sources driven by similar laser parameters^[26,37], after the THz pulse propagated $250\ \mu\text{m}$ off the plasma. Because the THz radiation comes from the wiggler process, the THz electric field waveform of multi-cycles^[51] was completely different from the half-cycle THz sources driven by intense lasers and plasma^[26,37,50].

2.4. Tunable frequency

From Figures 3(a) and 3(c), one can see that the electrons in group A had a large divergence angle. The electron density n_e decreases with the increase of transmission distance, and E_s becomes weaker for the longer plasma according to Equation (1), in which case the electrons in group B are more difficult to pull back to the plasma. As a result of enhancing l_p , l_s becomes larger and more electrons no longer participate in the wiggler motion. Hence, the center frequency decreases and the growth of energy conversion efficiency gradually slows down with the enhancement of l_p . Simulations by varying l_p from 50 to $900\ \mu\text{m}$ have demonstrated the effect on the center frequency, as shown in Figure 5(a). From the figure, one can see that the center frequency of the THz pulse was tunable from 3.5 to 2.6 THz by changing the plasma length l_p from 150 to $900\ \mu\text{m}$. On the other hand, the laser-THz energy conversion efficiency, which increased with l_p and became saturated after $600\ \mu\text{m}$, as shown in

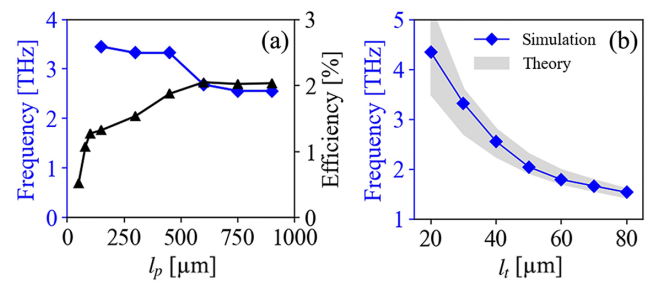


Figure 5. (a) The center frequency of the THz source and the laser-THz energy conversion efficiency from the simulations with plasmas of different lengths l_p from 50 to $900\ \mu\text{m}$, while l_t was fixed to $30\ \mu\text{m}$. (b) The center frequency of the THz source from the simulations (blue line) and the theoretical model of Equation (4) for the plasma thickness l_t changing from 20 to $80\ \mu\text{m}$ (light black shadow).

Figure 5(a), was 2.05%. The saturation length may be longer than $600\ \mu\text{m}$ since a small portion of the THz source came out of the simulation window, in the case of longer l_p , due to the limitation of computational ability.

Equation (4) indicates that we could regulate the center frequency of the THz pulse by changing the thickness of the plasma l_t . More simulations were performed by changing l_t from 20 to $80\ \mu\text{m}$ (fixed l_p at $300\ \mu\text{m}$). It was found that the laser-THz energy conversion efficiency was almost the same for different l_t , while the center frequency of the THz source decreased with the increase of l_t , as shown in Figure 5(b). For different l_t , ν_t can be obtained from the corresponding simulations, and the simulation results also show l_s ranging from 0.5 to $5\ \mu\text{m}$. We assumed that K decreased with the increase of l_s from 6.0 to 5.5 for the above cases, then we calculated the center frequencies of the THz pulse according to Equation (4) and plotted them in Figure 5(b). From the figure, one can see that the theoretical model developed here works very well in predicting the generation of center-frequency-tunable THz pulses with a laser-driven plasma wiggler.

3. Discussion

To validate the physical results, we conducted 3D PIC simulations using a box size of $1920 \times 800 \times 800$ and a resolution of $0.15\lambda \times 0.25\lambda \times 0.25\lambda$ (further details can be found in the Supplementary Material). The 3D simulation produced a spectrum in the cross-section that closely resembles that obtained from the 2D simulation. In addition, the spatial distribution exhibits a quasi-2D pattern, indicating similarities between the two simulations.

Parametric simulations were also carried out to see the effects of laser intensity, plasma density and density gradient at the boundary (more details in the Supplementary Material). It was found that the energy conversion efficiency was almost unchanged for the plasma of the same thickness

under a relativistic intense laser ($a_0 \geq 1.0$), while the center frequency, which decreased from 3.35 to 1.7 THz, would further reduce under smaller a_0 due to the drop of electron v_t . Since a low-density plasma is more beneficial to improving the energy efficiency from the laser pulse to relativistic electrons, the laser–THz energy conversion efficiency was higher in the case of lower density plasma. However, the center frequency of the THz source was almost the same. In reality, the plasma has a density gradient at the boundaries. Simulations using a pre-expand plasma with a scale length varied from 0.1 to 1 μm showed that there were almost no changes in the THz angular-spectra distribution. The parametric scans demonstrated the validity of this novel laser-driven plasma wiggler for the generation of high-power and center-frequency-tunable THz pulses over a wide range of laser and plasma parameters. With this method, one could produce ultra-high-power THz pulses of approximately 200 mJ by using a laser pulse of approximately 10 J. Such a state-of-the-art THz source would initiate future applications of high-power THz pulses based on a compact laser.

4. Conclusion

In summary, we propose a laser-driven plasma wiggler for efficiently generating a high-power, collimated, narrow-band and center-frequency-tunable THz pulse, by manipulating the electron reciprocating motion. A theoretical model is developed to describe the physical principle of realizing the center-frequency-tunable THz pulse. According to the model and PIC simulations, the center frequency of the THz pulse corresponds strictly to the reciprocating motion period of the electron beam. Simulations indicate that the center frequency of the THz pulses can be tuned from 4.4 to 1.5 THz as the plasma thickness changes from 20 to 80 μm . Meanwhile, the THz pulse is collimated into a divergence angle of approximately 20° , enabling a laser–THz conversion efficiency of more than 2.0% and an ultra-strong-field strength of over 80 GV/m, driven by a table-top laser of approximately 430 mJ. This method could address a long-standing challenge in THz science and generate a state-of-the-art THz source over a wide range of laser and plasma parameters.

Appendix A. Particle-in-cell simulation setup

Numerical simulations were performed by using the 2D PIC codes EPOCH^[52] and SMILEI^[53] to verify this scheme. The simulation window $X \times Y = 600 \mu\text{m} \times 570 \mu\text{m}$ was divided into $12,500 \times 7125$ cells. A laser pulse, with Gaussian spatial and \sin^2 temporal profiles, wavelength $\lambda_0 = 800 \text{ nm}$, waist $w_0 = 7.2 \mu\text{m}$, normalized intensity $a_0 = 3$, polarized in the Y direction and with the duration of 32 fs at FWHM, was used as the driving source. Such a laser pulse can be

produced by a compact laser^[54]. We used a block-shaped near-critical density plasma (electron density $n_e = 0.2n_c$, where n_c is the critical density) whose length and thickness were adjustable. Such a plasma could be made of carbon nanotube foams^[55,56]. Twenty-four (four) macro-electrons (C^{6+}) were initialized into each cell. The simulation time was varied with plasma length l_p to make sure that we had more than 1 picosecond to collect the THz signal, which should be enough to cover the whole interaction process for the generation of THz sources. Meanwhile, the zero padding method^[57] was used to further improve the resolution of the THz signal.

Acknowledgements

This work was supported by the National Natural Science Foundation of China (Grant Nos. 11921006 and 12175058), Beijing Distinguished Young Scientist Program and National Grand Instrument Project (Grant No. SQ2019YFF01014400). The PIC code EPOCH was in part funded by UK EPSRC (Grant Nos. EP/G054950/1, EP/G056803/1, EP/G055165/1 and EP/M022463/1). We give thanks for the helpful discussions with Prof. Z. Najmudin from Imperial College London and Prof. Wenjun Ma from Peking University.

Supplementary Material

To view supplementary material for this article, please visit <http://doi.org/10.1017/hpl.2023.78>.

References

1. P. H. Siegel, *IEEE Trans. Microwave Theory Techn.* **50**, 910 (2002).
2. C. Sirtori, *Nature* **417**, 132 (2002).
3. R. Ulbricht, E. Hendry, J. Shan, T. F. Heinz, and M. Bonn, *Rev. Mod. Phys.* **83**, 543 (2011).
4. W. J. Choi, G. Cheng, Z. Huang, S. Zhang, T. B. Norris, and N. A. Kotov, *Nat. Mater.* **18**, 820 (2019).
5. T. Kleine-Ostmann and T. Nagatsuma, *J. Infrared Millimeter Terahertz Waves* **32**, 143 (2011).
6. S. Koenig, D. Lopez-Diaz, J. Antes, F. Boes, R. Henneberger, A. Leuther, A. Tessmann, R. Schmogrow, D. Hillerkuss, R. Palmer, T. Zwick, C. Koos, W. Freude, O. Ambacher, J. Leuthold, and I. Kallfass, *Nat. Photonics* **7**, 977 (2013).
7. D. A. Kalashnikov, A. V. Paterova, S. P. Kulik, and L. A. Krivitsky, *Nat. Photonics* **10**, 98 (2016).
8. X. C. Zhang, A. Shkurinov, and Y. Zhang, *Nat. Photonics* **11**, 16 (2017).
9. R. F. Kazarinov and R. A. Suris, *Fiz. Tekh. Poluprovodn.* **5**, 797 (1971).
10. J. Faist, F. Capasso, D. L. Sivco, C. Sirtori, A. L. Hutchinson, and A. Y. Cho, *Science* **264**, 553 (1994).
11. K. H. Yang, P. L. Richards, and Y. R. Shen, *Appl. Phys. Lett.* **19**, 320 (1971).
12. D. H. Auston, K. P. Cheung, J. A. Valdmanis, and D. A. Kleinman, *Phys. Rev. Lett.* **53**, 1555 (1984).
13. D. H. Auston, K. P. Cheung, and P. R. Smith, *Appl. Phys. Lett.* **45**, 284 (1984).

14. A. Maestrini, J. S. Ward, J. J. Gill, H. S. Javadi, E. Schlecht, C. Tripon-Canselier, G. Chattopadhyay, and I. Mehdi, *IEEE Trans. Microwave Theory Techn.* **53**, 2835 (2005).
15. T. W. Crowe, R. J. Mattauch, H. P. Roser, W. L. Bishop, W. C. B. Peatman and X. Liu, *Proc. IEEE* **80**, 1827 (1992).
16. T. Kampfrath, K. Tanaka, and K. A. Nelson, *Nat. Photonics* **7**, 680 (2013).
17. J. L. LaRue, T. Katayama, A. Lindenberg, A. S. Fisher, H. Öström, A. Nilsson, and H. Ogasawara, *Phys. Rev. Lett.* **115**, 036103 (2015).
18. L. Zhao, Z. Wang, H. Tang, R. Wang, Y. Cheng, C. Lu, T. Jiang, P. Zhu, L. Hu, W. Song, H. Wang, J. Qiu, R. Kostin, C. Jing, S. Antipov, P. Wang, J. Qi, Y. Cheng, D. Xiang, and J. Zhang, *Phys. Rev. Lett.* **122**, 144801 (2019).
19. M. T. Hibberd, A. L. Healy, D. S. Lake, V. Georgiadis, E. J. H. Smith, O. J. Finlay, T. H. Pacey, J. K. Jones, Y. Saveliev, D. A. Walsh, E. W. Snedden, R. B. Appleby, G. Burt, D. M. Graham, and S. P. Jamison, *Nat. Photonics* **14**, 755 (2020).
20. D. Zhang, A. Fallahi, M. Hemmer, X. Wu, M. Fakhari, Y. Hua, H. Cankaya, A.-L. Calendron, L. E. Zapata, N. H. Matlis, and F. X. Kärtner, *Nat. Photonics* **12**, 336 (2018).
21. C. Lu, T. He, L. Zhang, H. Zhang, Y. Yao, S. Li, and S. Zhang, *Phys. Rev. A* **92**, 063850 (2015).
22. I. Babushkin, W. Kuehn, C. Koehler, S. Skupin, L. Berge, K. Reimann, M. Woerner, J. Herrmann, and T. Elsaesser, *Phys. Rev. Lett.*, **105**, 053903 (2010).
23. L. Bergé, K. Kaltenecker, S. Engelbrecht, A. Nguyen, S. Skupin, L. Merlat, B. Fischer, B. Zhou, I. Thiele, and P. U. Jepsen, *Europhys. Lett.* **126**, 24001 (2019).
24. H. Hamster, A. Sullivan, S. Gordon, W. White, and R. W. Falcone, *Phys. Rev. Lett.* **71**, 2725 (1993).
25. A. Gopal, S. Herzer, A. Schmidt, P. Singh, A. Reinhard, W. Ziegler, D. Brömmel, A. Karmakar, P. Gibbon, U. Dillner, T. May, H.-G. Meyer, and G. G. Paulus, *Phys. Rev. Lett.* **111**, 074802 (2013).
26. L. Yi and T. Fülöp, *Phys. Rev. Lett.* **123**, 094801 (2019).
27. C. Vicario, C. Ruchert, F. Ardana-Lamas, P. M. Derlet, B. Tudu, J. Luning, and C. P. Hauri, *Nat. Photonics* **7**, 720 (2013).
28. S. Baierl, M. Hohenleutner, T. Kampfrath, A. K. Zvezdin, A. V. Kimel, R. Huber, and R. V. Mikhaylovskiy, *Nat. Photonics* **10**, 715 (2016).
29. E. Balogh, K. Kovacs, P. Dombi, J. A. Fulop, G. Farkas, J. Hebling, V. Tosa, and K. Varju, *Phys. Rev. A* **84**, 023806 (2011).
30. K.-J. Yuan and A. D. Bandrauk, *Phys. Rev. Lett.* **110**, 023003 (2013).
31. A. D. Koulouklidis, C. Gollner, V. Shumakova, V. Y. Fedorov, A. Pugžlys, A. Baltuška, and S. Tzortzakis, *Nat. Commun.* **11**, 292 (2020).
32. G. Liao, Y. Li, H. Liu, G. G. Scott, D. Neely, Y. Zhang, B. Zhu, Z. Zhang, C. Armstrong, E. Zemaityte, P. Bradford, P. G. Huggard, D. R. Rusby, P. McKenna, C. M. Brenner, N. C. Woolsey, W. Wang, Z. Sheng, and J. Zhang, *Proc. Natl. Acad. Sci.* **116**, 3994 (2019).
33. A. J. Pearson, J. Palastro, and T. M. Antonsen, *Phys. Rev. E* **83**, 056403 (2011).
34. C. Miao, J. P. Palastro, and T. M. Antonsen, *Phys. Plasmas* **24**, 043109 (2017).
35. K. B. Kwon, T. Kang, H. S. Song, Y.-K. Kim, B. Ersfeld, D. A. Jaroszynski, and M. S. Hur, *Sci. Rep.* **8**, 145 (2018).
36. D. N. Gupta, A. Jain, V. V. Kulagin, M. S. Hur, and H. Suk, *Appl. Phys. B* **128**, 50 (2022).
37. G.-Q. Liao, H. Liu, G. G. Scott, Y.-H. Zhang, B.-J. Zhu, Z. Zhang, Y.-T. Li, C. Armstrong, E. Zemaityte, P. Bradford, D. R. Rusby, D. Neely, P. G. Huggard, P. McKenna, C. M. Brenner, N. C. Woolsey, W.-M. Wang, Z.-M. Sheng, and J. Zhang, *Phys. Rev. X* **10**, 031062 (2020).
38. G.-Q. Liao and Y.-T. Li, *IEEE Trans. Plasma Sci.* **47**, 3002 (2019).
39. S. C. Wilks, W. L. Kruer, M. Tabak, and A. B. Langdon, *Phys. Rev. Lett.* **69**, 1383 (1992).
40. H. Daido, M. Nishiuchi, and A. S. Pirozhkov, *Rep. Progress Phys.* **75**, 056401 (2012).
41. R. Tarkeshian, J. L. Vay, R. Lehe, C. B. Schroeder, E. H. Esarey, T. Feurer, and W. P. Leemans, *Phys. Rev. X* **8**, 021039 (2018).
42. Y. Sentoku, T. E. Cowan, A. Kemp, and H. Ruhl, *Phys. Plasmas* **10**, 2009 (2003).
43. P. Mora, *Phys. Rev. Lett.* **90**, 185002 (2003).
44. Y. T. Li, X. H. Yuan, M. H. Xu, Z. Y. Zheng, Z. M. Sheng, M. Chen, Y. Y. Ma, W. X. Liang, Q. Z. Yu, Y. Zhang, F. Liu, Z. H. Wang, Z. Y. Wei, W. Zhao, Z. Jin, and J. Zhang, *Phys. Rev. Lett.* **96**, 165003 (2006).
45. D. H. Bilderback, P. Elleaume, and E. Weckert, *J. Phys. B* **38**, S773 (2005).
46. J. D. Jackson, *Classical Electrodynamics* (American Association of Physics Teachers, 1999).
47. J. Cai, Y. R. Shou, L. Q. Han, R. X. Huang, Y. X. Wang, Z. H. Song, Y. X. Geng, J. Q. Yu, and X. Q. Yan, *Opt. Lett.* **47**, 1658 (2022).
48. É. Lalor, *J. Opt. Soc. Am.* **58**, 1235 (1968).
49. A. Ritter, *Opt. Express* **22**, 26265 (2014).
50. G. Q. Liao, Y. T. Li, C. Li, L. N. Su, Y. Zheng, M. Liu, W. M. Wang, Z. D. Hu, W. C. Yan, J. Dunn, J. Nilsen, J. Hunter, Y. Liu, X. Wang, L. M. Chen, J. L. Ma, X. Lu, Z. Jin, R. Kodama, Z. M. Sheng, and J. Zhang, *Phys. Rev. Lett.* **114**, 255001 (2015).
51. Y. Tian, J. Liu, Y. Bai, S. Zhou, H. Sun, W. Liu, J. Zhao, R. Li, and Z. Xu, *Nat. Photonics* **11**, 242 (2017).
52. T. D. Arber, K. Bennett, C. S. Brady, A. Lawrence-Douglas, M. G. Ramsay, N. J. Sircombe, P. Gillies, R. G. Evans, H. Schmitz, A. R. Bell, and C. P. Ridgers, *Plasma Phys. Contr. Fusion* **57**, 113001 (2015).
53. J. Derouillat, A. Beck, F. Pérez, T. Vinci, M. Chiaramello, A. Grassi, M. Flé, G. Bouchard, I. Plotnikov, N. Aunai, J. Dargent, C. Riconda, and M. Grech, *Comput. Phys. Commun.* **222**, 351 (2018).
54. C. N. Danson, C. Haefner, J. Bromage, T. Butcher, J.-C. F. Chanteloup, E. A. Chowdhury, A. Galvanauskas, L. A. Gizzi, J. Hein, D. I. Hillier, N. W. Hopps, Y. Kato, E. A. Khazanov, R. Kodama, G. Korn, R. Li, Y. Li, J. Limpert, J. Ma, C. H. Nam, D. Neely, D. Papadopoulos, R. R. Penman, L. Qian, J. J. Rocca, A. A. Shaykin, C. W. Siders, C. Spindloe, S. Szatmári, R. M. G. M. Trines, J. Zhu, P. Zhu, and J. D. Zuegel, *High Power Laser Sci. Eng.* **7**, e54 (2019).
55. W. Ma, L. Song, R. Yang, T. Zhang, Y. Zhao, L. Sun, Y. Ren, D. Liu, M. Liu, J. Shen, Z. Zhang, Y. Xiang, W. Zhou, and S. Xie, *Nano Lett.* **7**, 2307 (2007).
56. Y. Shou, P. Wang, S. G. Lee, Y. J. Rhee, H. W. Lee, J. W. Yoon, J. H. Sung, S. K. Lee, Z. Pan, D. Kong, Z. Mei, J. Liu, S. Xu, Z. Deng, W. Zhou, T. Tajima, I. W. Choi, X. Yan, C. H. Nam, and W. Ma, *Nat. Photonics* **17**, 137 (2023).
57. C. R. Harris, K. J. Millman, S. J. Van Der Walt, R. Gommers, P. Virtanen, D. Cournapeau, E. Wieser, J. Taylor, S. Berg, N. J. Smith, R. Kern, M. Picus, S. Hoyer, M. H. van Kerkwijk, M. Brett, A. Haldane, J. F. del Río, M. Wiebe, P. Peterson, P. Gérard-Marchant, K. Sheppard, T. Reddy, W. Weckesser, H. Abbasi, C. Gohlke, and T. E. Oliphant, *Nature* **585**, 357 (2020).